ADVANCED MATERIALS

Supporting Information

for *Adv. Mater.*, DOI: 10.1002/adma. 201504740

Dynamic Behavior in Enzyme–Polymer Surfactant Hydrogel Films

*Kamendra P. Sharma, Robert Harniman, Thomas Farrugia, Wuge H. Briscoe, Adam W. Perriman, and Stephen Mann**

Supporting Information

Dynamic Behaviour in Enzyme-Polymer Surfactant Hydrogel Films

*Kamendra P. Sharma, Robert Harniman, Thomas Farrugia, Wuge H. Briscoe, Adam W. Perriman, and Stephen Mann**

Table of Contents:

1. Experimental:

(a) Materials:

Alkaline Phosphatase from bovine intestinal mucosa (P7640; ≥ 3.3 glycine units mg^{-1} solid), myoglobin from equine skeletal muscle (95-100%, lyophilized powder; Mb; M0630), ferritin from equine spleen (F4503; type I saline solution), Glucose oxidase (Aspergillus niger (G7141); type X-S, activity 100 000−250 000 units/g solid (without added oxygen)), 3-dimethylamino propylamine (DMAPA; D14500-9), N-(3-dimethylaminopropyl)-N′-ethylcarbodiimide hydrochloride (EDC; E7750), Poly(ethylene glycol) 4-nonylphenyl 3-sulfopropyl ether potassium salt (C_9H_{19}-C_6H_4-$(OCH_2CH_2)_{19}O(CH_2)_3SO_3^-$ K^+; M_n= 1197; PDI=1.03 (**S1**; 473197), sodium bis-2-ethylhexyl sulphosuccinate (AOT; 86139), phosphatase substrate,4-nitrophenyl phosphate disodium salt hexahydrate (*p*NPP; P4744), and rhodamine B (RHB; R6626) were all purchased from Sigma-Aldrich and used as received. Enhanced green fluorescent protein (EGFP) was expressed in E. coli BL21(DE3) from the plasmid vector pET45b(+) (Novagen, Germany), and purification was achieved via polyhistidine tag using metal ion affinity [Ni-NTA (Qiagen)] chromatography.

(b) Instrumentation:

AFM measurements were conducted on two versions of multi-mode microscope (Bruker). Tapping mode imaging was performed using a multi-mode V system utilising a silicon cantilever of nominal stiffness 50 N/m and fundamental resonance 300 kHz (ACT-25 AppNano). PeakForce imaging was performed using a multi-mode VIII system utilising a silicon cantilever of nominal stiffness 0.4 N/m and fundamental resonance 130 kHz (SCANASYST-AIR_HR Bruker). The films were imaged at ambient temperature, both in dry and hydrated state. The same cantilever was used over the same sample both dry and after wetting. To hydrate the film, the cantilever was removed and 100 µL of distilled deionized water was added via a micropipette until the theoretical saturation point of the film was reached. At this point the film has absorbed the added liquid and interacted with it without an additional liquid layer remaining on the surface of the film. This level of saturation was maintained through significantly increasing the relative humidity local to the sample. In the first two minutes after hydration significant drift is observed in the AFM imaging due to the swelling and rearrangement of the film. After this point the image remains stable over large time-scales suggesting re-arrangement has finished and the film is in a stable hydrated state. The image measurements were averaged over ten examples of the most protruding clusters from each

sample. SAXS and WAXS experiments were performed on a GANESHA 300XL+ system equipped with a X-ray Generator and Genix 3D Cu-source with integrated monochromator (multilayer optic "3D version" optimized for SAXS). Collimator section was made up of three motorized 4-blade slits containing high polished single crystal blades for minimal slit-scatter (allowing for a factor of 1000 in *q*-range (3E-3 $Å^{-1}$ to $3Å^{-1}$)). Large sample chamber with large fast-entry door contained a sample Stage that could be translated in Y and Z direction and also had rotational capabilities. Coarse positioning of the sample along the beam flight path could be done using a camera viewer inside the sample chamber. A positioning stage provided 2D positioning of a Pilatus detector (300K- 20 Hz) and thus variable sample-to-detector distances (from 120 mm to 1400 mm). The dry [cALP-**S_1**] was grounded into small pieces and then filled into 1.5 mm diameter quartz glass capillaries tubes. The tubes were then filled with the desired solvent and sealed with araldite. After sealing the films in the capillaries were allowed to be saturated with the solvent for 30 minutes before putting characterizing with SAXS. Thermal gravimetric analyses (TGA) measurements were done to determine the amount of water uptake by a saturated [cALP-**S_1**] film on a TA Q500 instrument using a Pt pan between 25 °C and 200 °C. The film was first dipped in water and then vigorously flicked couple of times by holding it within tweezers to remove excess water before putting it on a Pt pan. The amount of water was determined by holding the TGA machine temperature at 110 °C for 1 hr and determining the weight change. Dynamic light scattering (DLS) measurements of the aqueous protein dispersions were performed on a Malvern Zetasizer Nano-ZS at a concentration of ≈ 0.5 - 1 mg cm^{-3}. Rheological measurements on the wet films were undertaken at room temperature using a Malvern Kinexus Pro+ rheometer. The geometry used was a 20 mm cone and plate and the gap between the mobile plate and the stationary base plate was set to 0.10 mm for all experiments. Oscillatory amplitude sweeps at 1 $rads^{-1}$ and 25°C were initially performed to determine the percentage strain from the linear viscoelastic region for frequency sweep measurements. Elastic modulus G′ and viscous modulus G″ were then plotted as a function of frequency to determine the viscoelastic properties of the wet [cALP-**S_1**] film. Diffuse UV-Vis (DR-UV-Vis) was performed on Perkin-Elmer Lambda 35 equipped with a Labsphere RSA-PE-20 diffuse reflectance detector. Field emission gun scanning electron microscopy (FEG-SEM) was performed on a JEOL Field Emission Gun SEM 6330 to examine the microstructure of the hybrid films. The sample for imaging was prepared by drying a wet [cALP-**S_1**] film onto a silicon wafer fixed with a carbon tape on an aluminum SEM stub, which was then sputtered with a 15 nm Ag layer to provide a conduction layer.

(c) Fabrication of protein-polymer surfactant bioconjugates and hybrid films:

Bioconjugate and nanocluster preparation: Native proteins (alkaline phosphatase (ALP), ferritin (Fn), myoglobin (Mb), enhanced green fluorescent protein (EGFP), or glucose oxidase (GOx)) were cationized by covalent coupling of glutamic and aspartic acid residues with 3-dimethylamino propylamine (DMAPA) by addition of N-(3-dimethylaminopropyl)-N′-ethylcarbodiimide hydrochloride (EDC) to yield cationized alkaline phosphatase (cALP), cationized ferritin (cFn), cationized myoglobin (cMb), cationized enhanced green fluorescent protein (cEGFP), or cationized glucose oxidase (cGO_x). Briefly a 2 mL of 0.2 M solution of DMAPA was adjusted to pH 6 using HCl (6M), after which it was added to a 10 mL solution of 5 mg mL^{-1} of native protein dissolved in MilliQ 18.2 $M\Omega^{-1}$ cm^{-1} water. After this 100 mg of EDC was added to the mixture. The reaction was allowed to proceed overnight, and the pH was adjusted to 6 at hourly intervals for the first 3 hours. This step was followed by dialysis of the cationized protein against MilliQ grade water, with three water changes. Any aggregates that formed during the reaction or dialysis steps were removed by centrifugating the modified proteins at 5000 rpm for 10 mins. Cationization efficiency was determined using MALDI TOF mass spectrometry and used to determine the amount of polymer surfactant required to half neutralize the protein surface charge required for nanocluster formation. Formation of the protein-polymer surfactant conjugates was achieved by controlled addition of a 50 mg mL^{-1} solution of **S_1** at a steady rate of 100 µL min^{-1} using a syringe pump to a stirred solution of 10 ml of 5-10 g mL^{-1} cationized protein. Formation of the bioconjugates and their spontaneous association into nanoclusters at a 1 : 2 stoichiometry was associated with an increase in solution turbidity. The formation of clusters was visualized using digital photography as shown in **Movie S5**. The cluster size determination using DLS gave hydrodynamic diameters of ~ 100-200 nm for all the proteins under consideration.

Film preparation: Films of bioconjugate proteins were produced by dispensing solutions of the bioconjugate nanoclusters into polystyrene petri dishes, after which they were placed in a desiccator containing a petri dish filled with 5 wt.% glutaraldehyde and silica as desiccant. Drying was facilitated by application of a 25 mm Hg vacuum to the desiccator. Overnight drying and vaporous glutaraldehyde crosslinking of the protein-polymer surfactant nanoconjugate clusters yielded self-standing films which were labelled as [cALP-**S_1**], [cFn-**S_1**], [cMb-**S_1**], [cEGFP-**S_1**], or [cGOx-**S_1**]. The resulting self-standing, crosslinked films were removed from the petri-dish by the addition of MilliQ grade water, which resulted in swelling of the film and buckling instabilities that resulted in delamination from the polystyrene dish. The SEM of the dry films (**Figure S1 and S18**) revealed a microstructure which comprised

crosslinked micron-sized particles assembled from few hundred nanometer sized clusters. A glassy and brittle fry [cFn-**S₁**] hybrid film also revealed an intact quaternary structure when microtomed by embedding in an epoxy resin and subjected to EDAX measurements on TEM (**Figure S19**).

(d) Water-in-oil microemulsion experiments:

Typically, 50 mg of solid sodium bis(2-ethylhexyl) sulfosuccinate (AOT) and 200 µL of 100 mM *p*NPP aqueous solution were added to 5 mL of iso-octane (2,2,4-trimethylpentane) to produce water-in-oil microemulsion droplets. The mixture was thoroughly vortexed to form a microemulsion with a molar ratio of $w \approx 100$; (w= [H_2O]/[AOT]). Using a linear relationship between the radius of the aqueous droplets (R_w) and w, a theoretical radius of the water pool was calculated as R_w = 15 nm (0.15w).[1] A dry and folded [cALP-**S₁**] film (~ 5mg) was then lowered into the vial containing the microemulsion using tweezers and dephosphorylation of *p*-nitrophenyl phosphate (*p*NPP) to *p*-nitro phenol (*p*NP) was monitored using snapshots from a digital camera over 10-15 minutes. For the dye uptake experiments, the *p*NPP aqueous solution was replaced by 50 µL of 1 mM rhodamine B dye aqueous solution providing a microemulsion with $w \approx 25$ and water pool radius, R_w = 3.75 nm.

2. Calculation of Elastic and Interfacial Surface Energies:

Approximating an irregular shaped completely unfolded film as a very thin circular sheet of radius *R* and thickness *t* being crumpled into a small ball like object of radius *r*, there are two competing energies involved in the auto-spreading/self-folding behaviour.

(a) Crumpling/elastic energy:

$$E_{crumpling} = Y\, t\, R^2 \left[\frac{t}{r}\right]^{5/3} \text{----------(1)}$$

where *Y* is the Young's modulus of the film, *t* is the thickness in μm, *R* is the size in cm, and R is the confinement radius of the film.

(b) Surface interfacial energy gain:

$$E_\gamma = \gamma \times \Delta A \text{----------(2)}$$

where γ is the surface tension and ΔA is the change in the overall surface area of the film.

Now $\Delta A = A_i - A_f$; i.e. the surface area before crumpling – after crumpling.

$$A_i = 2\pi R^2 + 4\pi Rt$$

$$A_f = 4\pi r^2$$

Therefore,

$$\Delta A \approx 2\pi R^2 - 4\pi r^2 \text{----------(3)}$$

the second term in A_i has been neglected as it is very small)

Now,

The Young's modulus, *Y*, can be calculated by the relation,

$$Y = 2G(1+\upsilon) \text{----------(4)}$$

where υ is Poisson's ratio, and *G* is the shear modulus obtained from rheology measurements. Assuming the films to be comprised of isotropic incompressible material, the value of υ can be taken as 0.5, which gives $Y \approx 6000$ Pa.

Therefore, for a film with, $t = 100$ μm, $R = 1$ cm, and $r = 1.5$ mm using equations 1 and 4:

$$E_{crumpling} = 6000 \times 10^{-4} \times (10^{-2})^2 \times [10^{-4}/(1.5 \times 10^{-3})]^{5/3}$$

$$= 6.57 \times 10^{-7} \text{ J}$$

Similarly equations (2) and (3) yield:

$$E_\gamma = \gamma \times \Delta A = 72 \times 10^{-3} \times [2\pi(10^{-2})^2 - 4\pi(1.5\times10^{-3})^2]$$

$$= 4.31\times 10^{-5}\ \text{J}$$

Clearly E_γ is 2 orders of magnitude greater than $E_{\text{crumpling}}$.

Now, for a critical thickness, t_c, where no folding occurs

$$E_{\text{crumpling}} = E_\gamma$$

$$Y\, t_c\, R^2 \left[\frac{t_c}{r}\right]^{5/3} = E_\gamma = \gamma \times \Delta A$$

$$Y\, t_c\, R^2 \left[\frac{t_c}{r}\right]^{5/3} = \gamma \times [2\pi R^2 + 4\pi R t_c - 4\pi r^2]$$

A graphical solution (**Figure S17**) of such an equation gives the value of t_c, as mentioned below in the table:

R (cm)	***R (mm)***	***Y (Pa)***	***t_c (μm)***
1.0	1.5	6000	500
1.0	2.5	6000	675
1.0	3.5	6000	800
2.0	3.5	6000	850

This suggests that the t_c strongly depends on the confinement radius, r, and the size of the film, R.

3. Supporting Figures:

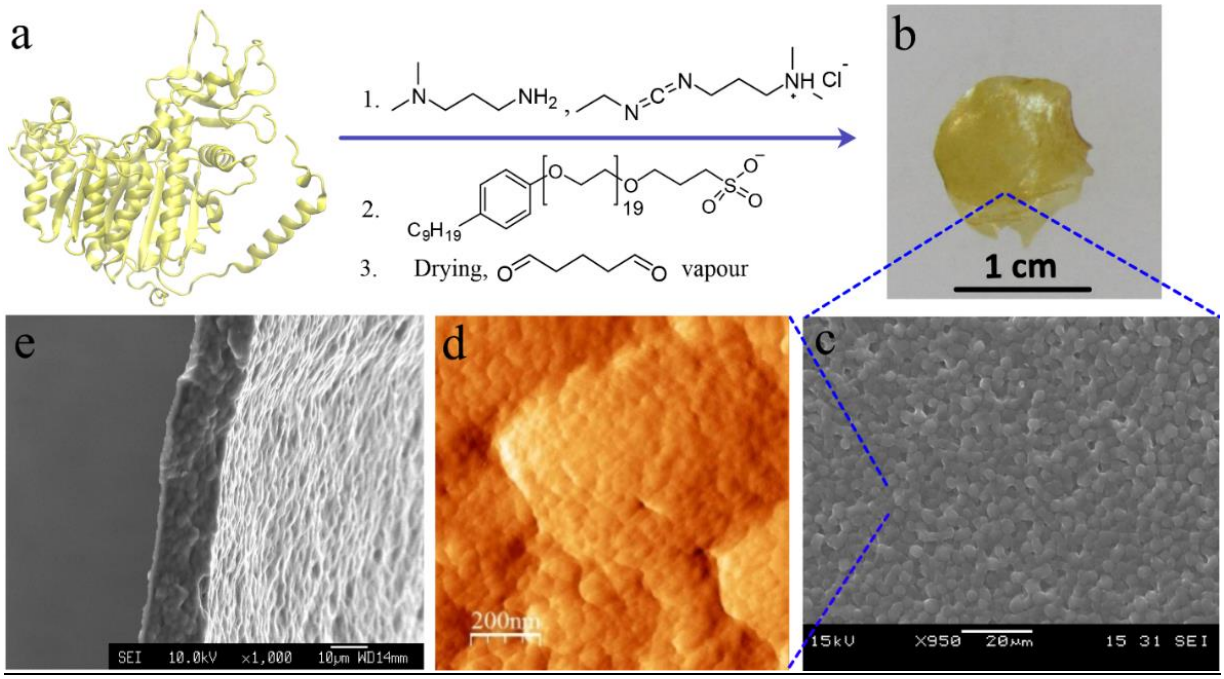

Figure S1: Synthesis of self-standing protein-polymer surfactant film: The process involves three steps: (1) cationisation of the glutamic and aspartic amino acid residues of the side chains at the surface of the protein, for e.g., alkaline phosphatase as shown here in **(a)**, with a diamine in the presence of EDC cross-linker; (2) addition of polymer surfactant resulting in the formation of protein-polymer surfactant clusters; (3) drying in a desiccator of a hybrid cluster solution in the presence of vapour glutaraldehyde to yield a self-standing [cALP-**S**$_1$] film. Image in **(b)** shows an example of hybrid [cALP-**S**$_1$] film after removal from the petri dish with water and subsequent drying. FEG-SEM was used to determine the morphology and the thickness of the film. The electron micrograph in **Figure (c)**, shows that the film comprised of cross-linked 2-3 micron-sized particles; higher resolution investigation of an AFM amplitude signal image reveals that the micron-sized particles are formed by self-assembly of nanometre size clusters **(d)**, suggesting the presence of a fractal like structure. The same film was tilted in the scanning electron microscope by 45 ° to determine its thickness as shown in **(e)**. The film was formed 4-5 of layers of micron size particles to give an overall thickness of 10-15 µm.

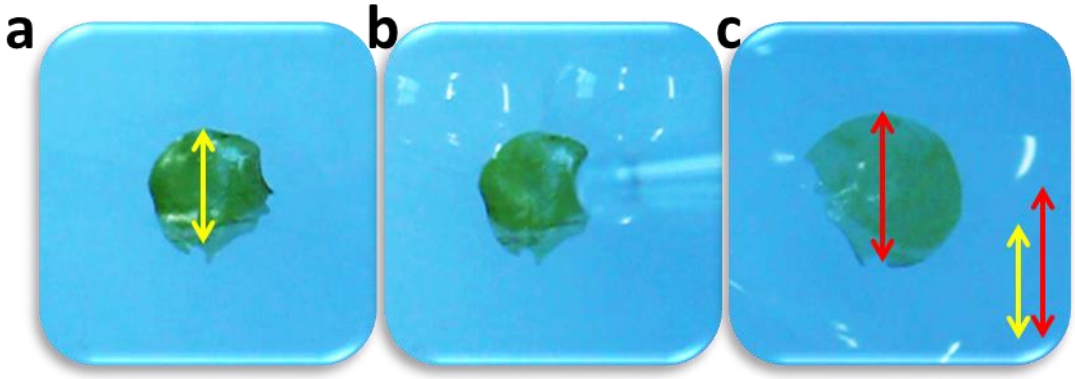

Figure S2: A detached ~ 100 µm thick [cALP-**S₁**] dry film showed an approximate 30% increase in diameter from 1 cm to 1.31 cm as the swelling was complete upon hydration. The yellow arrow shows diameter when dry and the red shows when completely wet. A comparison of the size of yellow and red arrows in panel [c] shows the extent of increase in diameter.

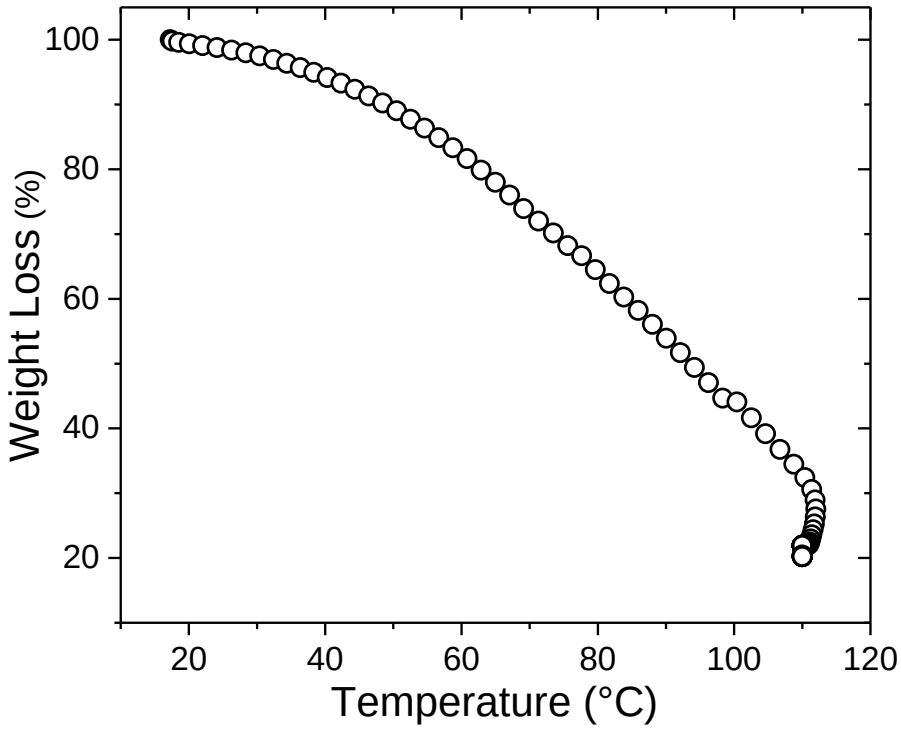

Figure S3: Thermal gravimetric analysis of [cALP-**S₁]** film after complete hydration and removal of excess water by shaking. The water content of the wet film is ~80 wt% of its hydrated mass.

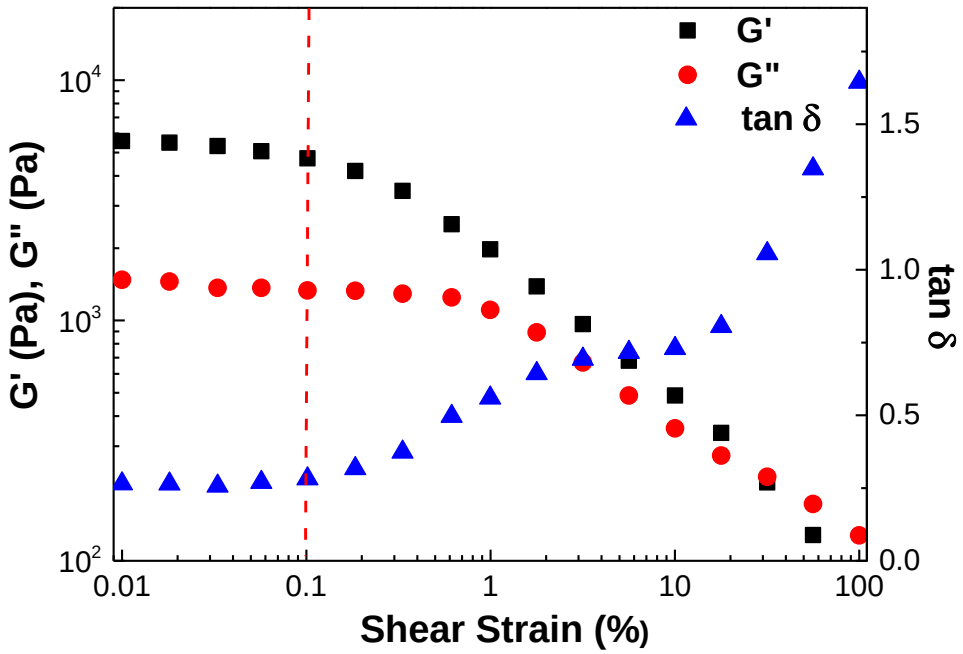

Figure S4: Amplitude strain sweep experiments for finding the linear viscoelastic region.

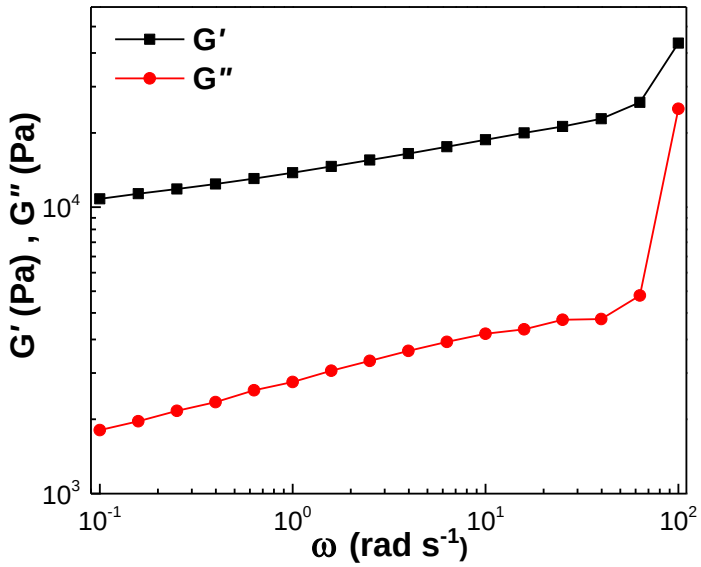

Figure S5: Rheological responses for a hydrated solution based glutaraldehyde crosslinked [cALP-**S1**] film exhibiting hydrogel properties. Dynamic frequency sweep of a wet [cALP-**S1**] film over a 0.01 to 100 rad s^{-1} and 0.1% strain at 25°C showing *ca.* 1.07 x 10^4 Pa.

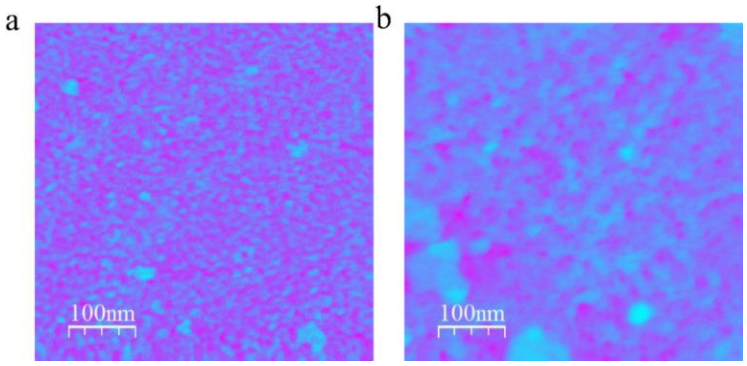

Figure S6a: AFM dissipation images of [cALP-**S₁**] film: The addition of water increases the size of the nanoclusters as seen by comparing dry (a) and hydrated (b) states of the film. The dissipation images seen for [cALP-**S₁**] film deliver an estimate of total energy transfer between the cantilever tip and the sample. In tapping mode this can be calculated from the phase angle of the cantilevers driven vibration. Dissipation data collected via PeakForce QNM and phase data collected via tapping mode are therefore qualitatively comparable. Analysis of the QNM surface stiffness and adhesion data comprising the dissipation supports the conclusion of the tapping mode data that the phase separation seen in the wet phase is indicative of a soft hydrated corona surrounding a stiffer core.

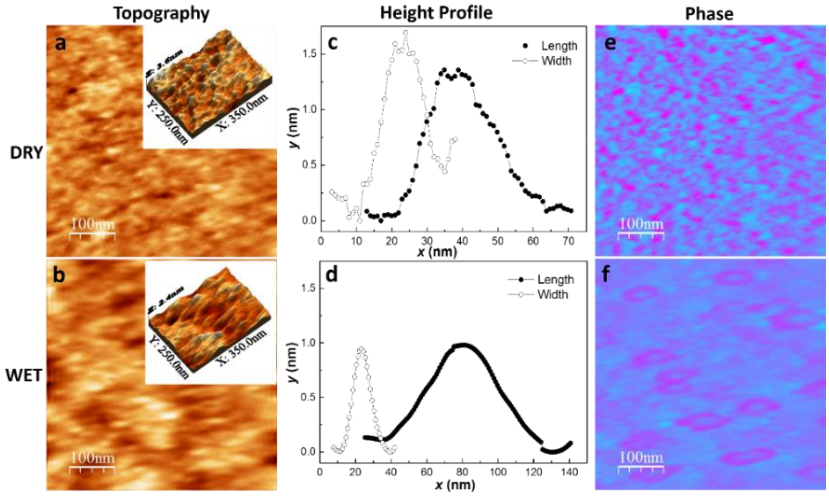

Figure S6b: AFM data for a [cGOx-**S₁**] film: Topography 2D (a, b) and 3D (*insets* in a, and b) data for the film in dry and water saturated state. The topography shows a change in the size of clusters upon saturation with water. The representative line profiles averaged over 10 clusters are shown in (c) and (d) for the dry and wet state of the film, respectively. Line profile showing the increase in length and width of the anisotropic clusters upon hydration, length increasing from 42 ± 3 nm to 92 ± 11 nm, while width increases from 17 ± 2 nm to 23 ± 2 nm. Phase contrast for the corresponding topography is shown in (e, f); phase separation is evident upon saturation where the outer and inner regions of clusters present differing phase contrast.

Figure S7: Detailed parameters from the poly core-shell model fit for the SAXS data of dilute [cALP-**S₁**] discrete nanoconjugates (below): The poly core shell model gives the form factor for polydisperse spherical particles with a core-shell structure. The sample for form factor analysis had a protein concentration of *ca.*1.3 mg mL^{-1} and was obtained by taking the supernatant after centrifuging the nanocluster solution at 8000 rpm for 15 minutes.

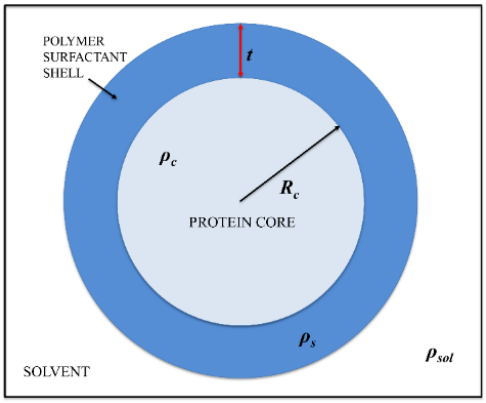

Parameters	**Values**
Scale	0.000528±1.2E-05
Avg. core radius, R_c (Å)	24.2
Avg. shell thickness, t (Å)	15.1
Overall polydispersity	0.19
SLD core, ρ_c ($Å^{-2}$)	1.37E-05
SLD shell, ρ_s ($Å^{-2}$)	1.18E-05
SLD solvent, ρ_{sol} ($Å^{-2}$)	9.469E-06
Incoherent background (cm^{-1})	0.0035

The model is given as follows:

$$F(q) = \frac{\text{Scaling}}{V_s} \times \left[\frac{3 \times V_c(\rho_c - \rho_s)\ K(qR_c)}{qR_c} + \frac{3 \times V_s(\rho_s - \rho_{sol})\ K(qR_s)}{qR_s} \right]^2 + background$$

where, $K(x) = \frac{Sinx - x\cos x}{x^2}, R_s = R_c + t, \text{and } V_y = 4/3\,\pi R_y^3)$

Apparent structure factors, $S_{app}(q)$, were calculated for the [cALP-**S₁**] film when dry or immersed in different solvents by dividing each scattering profile (solid lines, **Figure 2d** in the main text) with the $F(q)$ profile (black circles, **Figure 2d** in the main text).The peaks obtained was fitted using an interference function for densely packed systems given by

$$S_{app}(q) = A/[1 + B \text{ x } F(q)]$$

where A is a constant, and B the packing factor.

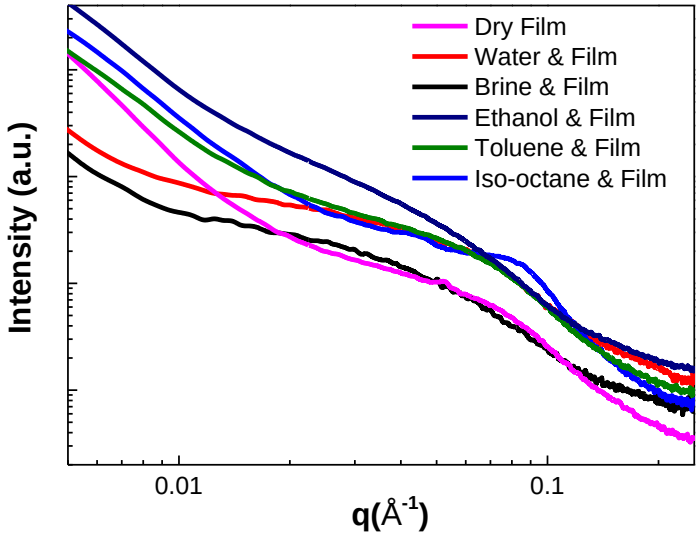

Figure S8: SAXS profiles for [cALP-**S**$_1$] film in different solvents: This data suggests that the swelling associated with hydrogel formation in the cross-linked films might be primarily driven by polar and not electrostatic interactions, presumably involving the poly(ethylene glycol) domains of the polymer surfactant molecules.

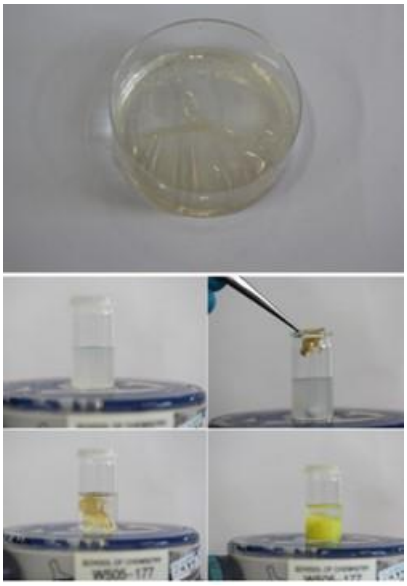

Figure S9: Water based enzymatic switch comprising [cALP-**S**$_1$] film and pNPP containing micro-emulsion: The top shows a wet [cALP-**S**$_1$] film. The dry [cALP-**S**$_1$] film when dipped in the form of a dry compact brownish globule absorbs water and *p*NPP within the first 60 s of immersion in the micro-emulsion, expands and develops slight yellow colour. After 10-15 minutes all the substrate has completely reacted with the film which now looks like a yellowish soft solid.

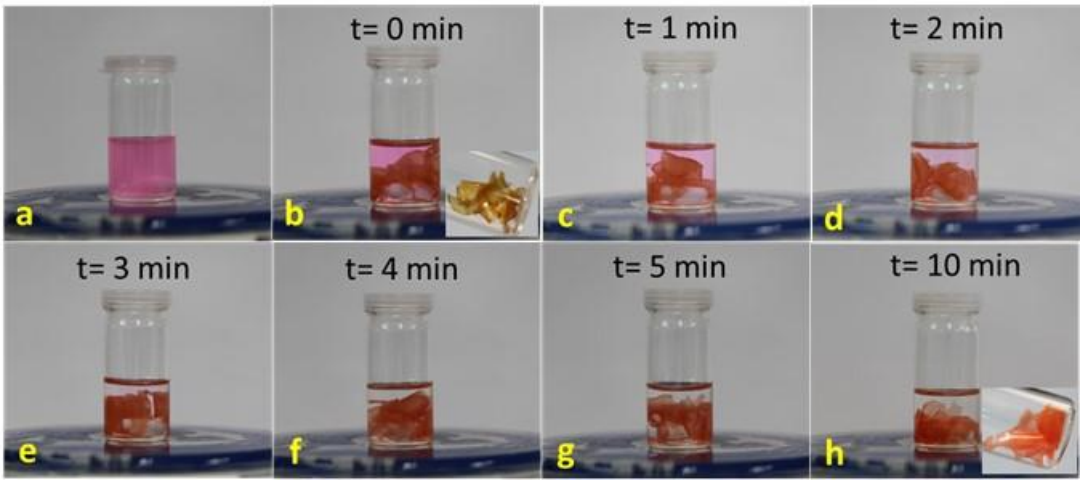

Figure S10: Dye uptake by [cALP-**S**$_1$] film from microemulsion: (a) Water in oil micro-emulsion droplets (100µL of 1 mM RHB aqueous solution, 100 mg NaAOT in 5 ml iso-octane). A dry [cALP- **S**$_1$**]** film is introduced in the micro-emulsion and stirred using a magnetic follower and the changes in colour observed over a period of 10 minutes (b-h). The insets in (b) and (h) shows the colour of the dried films before and after putting in the micro-emulsion solution. The change in colour from brown to pink is a result of dye absorbed by the film.

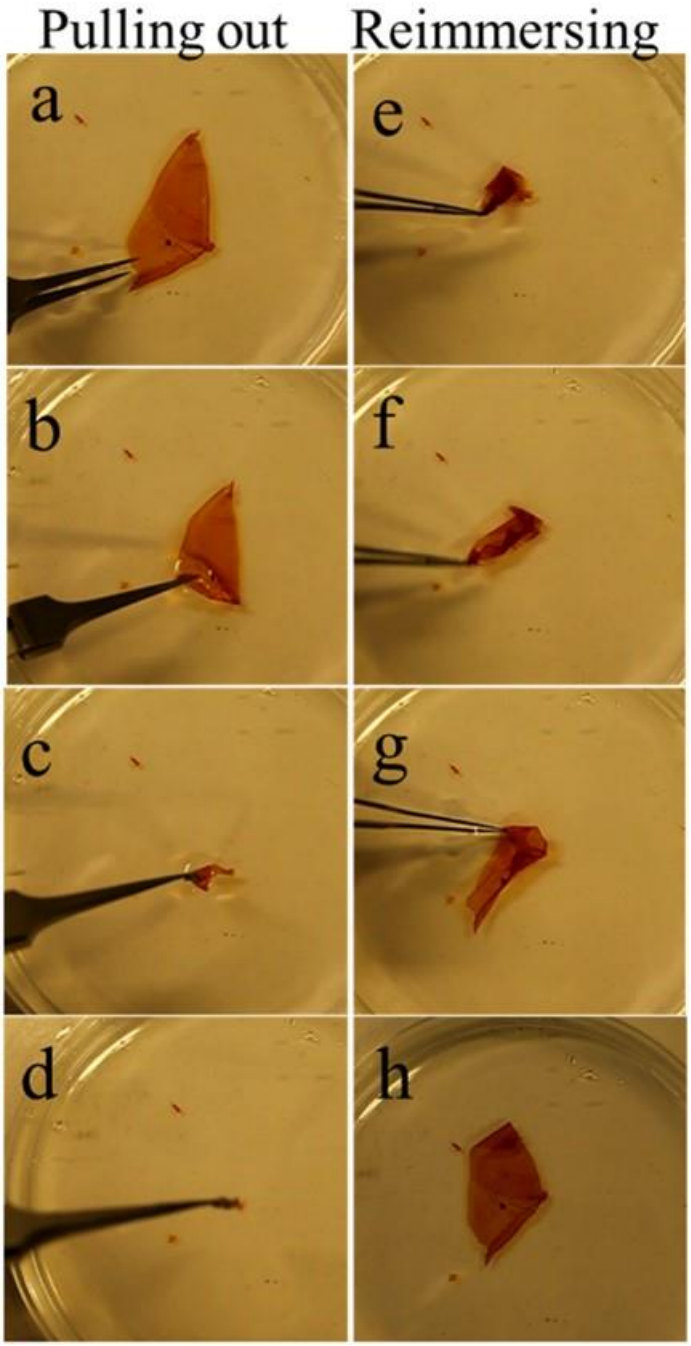

Figure S11: Reversible auto-spreading of [cFn-**S$_1$**] hybrid films: Time sequence of photographs showing a **[cFn-S$_1$]** hybrid film initially spread under water (t = 0) followed by removal/pulling out from the water phase to produce rapid crumpling of the film in air [(a) to (d); t = 0.07 to 0.58 s]. Re-immersion of the crumpled film into the water phase results in its instantaneous re-spreading without loss of structural integrity [(e) to (h); t = 0.81 to 4 s)]. The film images have been magnified for the purpose of clarity, thereby restricting the visibility of the complete water layer in the petri-dish.

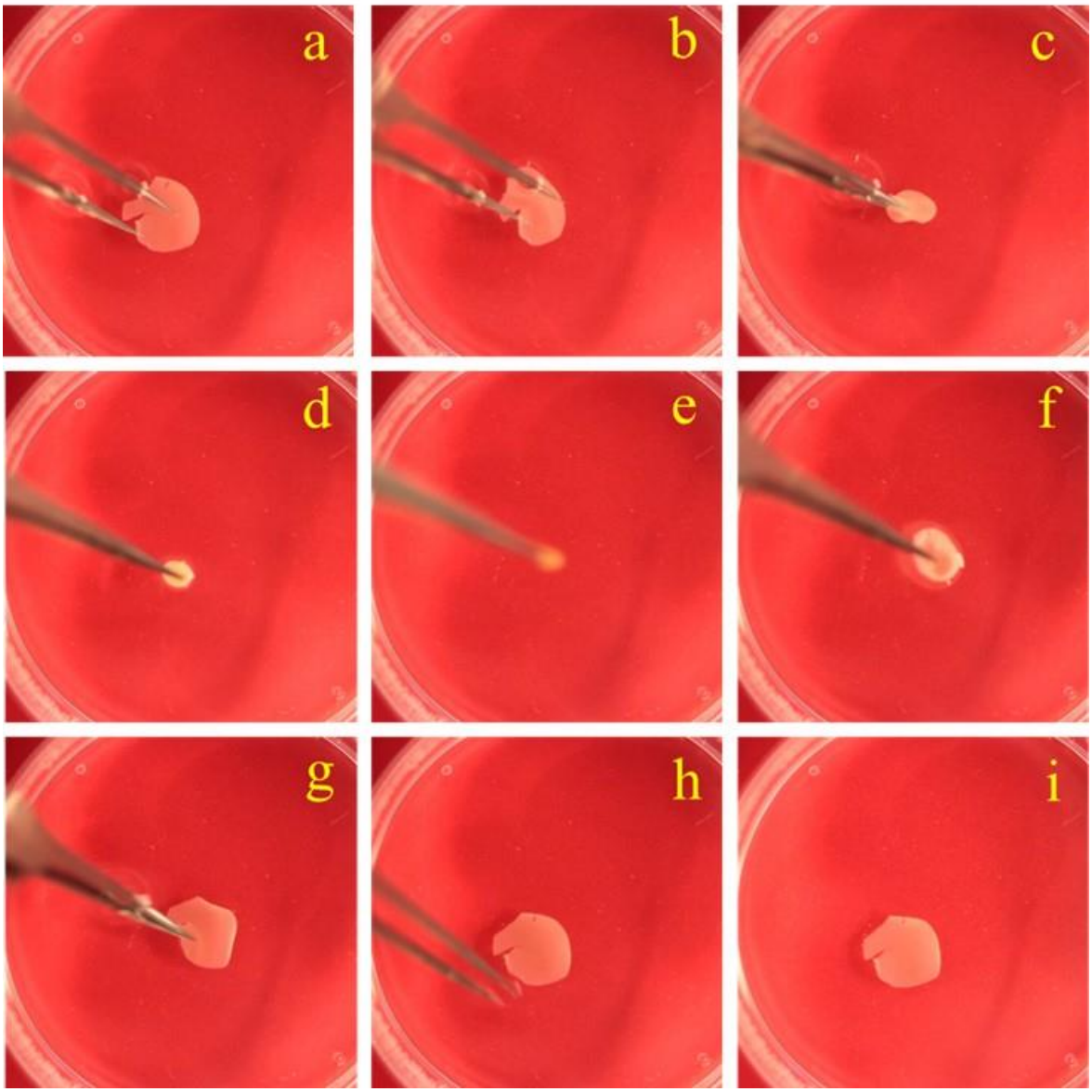

Figure S12: Reversible auto-spreading of [cALP-**S$_1$**] hybrid films: Time sequence of photographs showing a [cALP-**S$_1$**] hybrid film (shown as cream-coloured circular disk initially spread under water [(a); t = 0] followed by removal from the water phase to produce rapid crumpling of the film in air [(b) to (e); t = 0.52 to 0.67 s]. Re-immersion of the crumpled film into the water phase [(f); t = 1.0 s] results in its instantaneous re-spreading without loss of structural integrity [(f) to (i); t = 1.0 to 1.58 s]. The film images have been magnified for the purpose of clarity, thereby restricting the visibility of the complete water layer in the petri-dish.

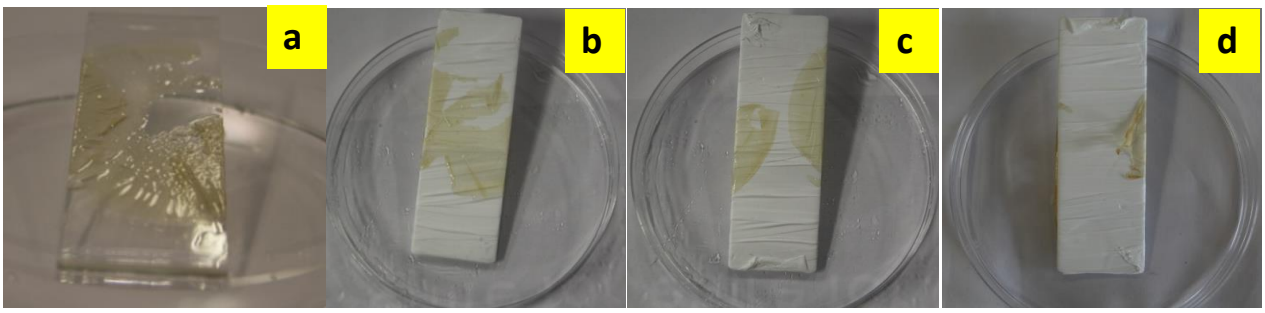

Figure S13: Snapshots of ~10 µm thick [cALP-S_1] film lifted from water onto a **(a)** bare glass slide (hydrophilic) or **(b)** teflon wrapped (hydrophobic) glass slide. The glass slide was placed below the hybrid film floating in water and then lifted; the wet hybrid film stuck to the surface of the glass slide (on bare or teflon wrapped) without collapsing. **(a)** The top side of the bare glass slide, **(b)** the top side of the teflon wrapped glass slide, **(c)** the back side of the glass slide shown in **(a)** with the hybrid film wrapping the teflon surface. **(c)** Snapshot of the same side as shown in **(c)** after the hybrid film has dried.

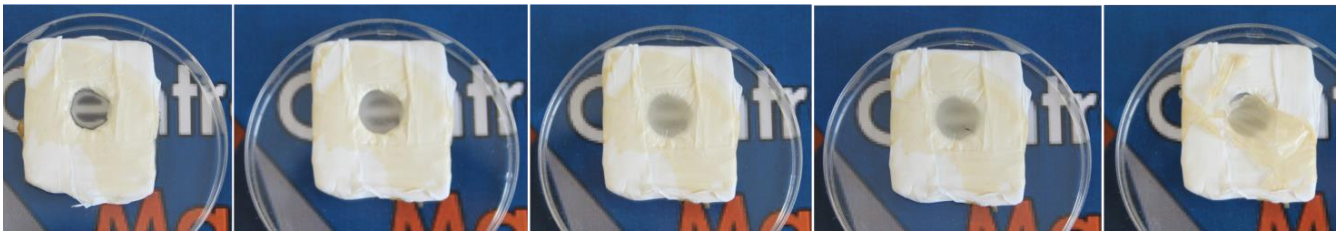

Figure S14: Snapshots of ~100 µm thick [cALP-S_1] film lifted from water using a teflon coated glass slide with a 8 mm orifice in centre. The snapshots were taken after every 10 minutes starting from the time as soon as it was taken out of water. The film when initially wet showed transparency (the letter "**e**" below the orifice can be seen clearly) but as it started drying it started turning opaque and after 30 minutes developed a crack due to stress in the 8 mm cavity (fourth snapshot). Finally after 50 minutes the entire film dried and started shrinking. The formation of opaqueness in the structure suggests the gel to solid transition.

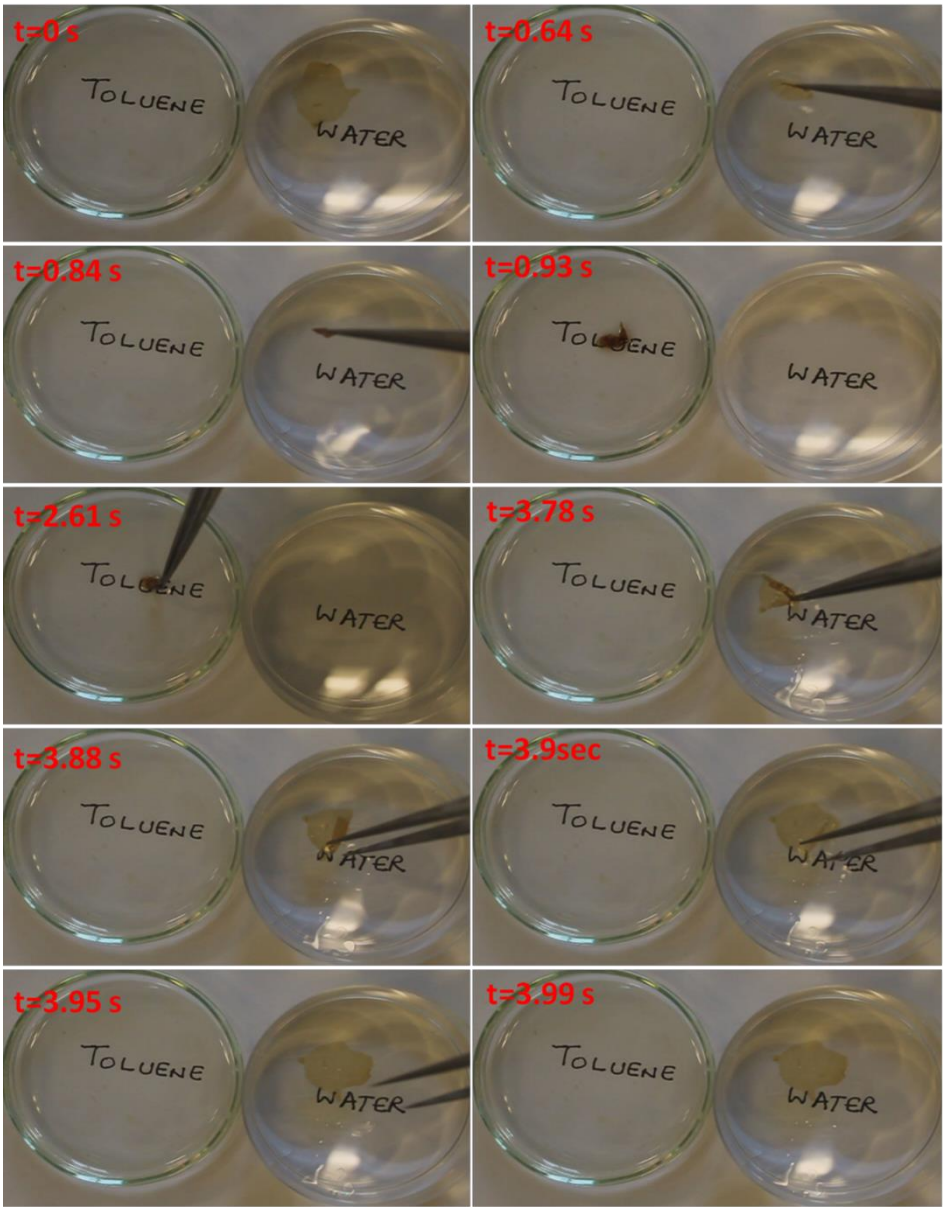

Figure S15: Structural behaviour of [cMb-**S₁**] hybrid film when transferred from water to toluene and back to water: Time sequence (**Movie S3**) shows [cMb-**S₁**] hybrid film initially spread in water (t = 0) followed by removal from the water phase to result in rapid crumpling of the film in air (t = 0.64 to 0.84 s). Immersion of the crumpled film in toluene (t = 0.93 s) does not result in auto-spreading process even after keeping the film in toluene for *ca.* 2 s. Removal of the crumpled film from toluene (at t = 2.61 s) and re-immersion in water results in instantaneous spreading of the film (t =3.78 to 3.99 s; toluene can be seen as an oil streak on the water surface). Similar self-folding/auto-spreading behaviour is seen for [cALP-**S₁**] film when transitioned from water (pink)→toluene→air→ toluene→water (**Movie S4**).

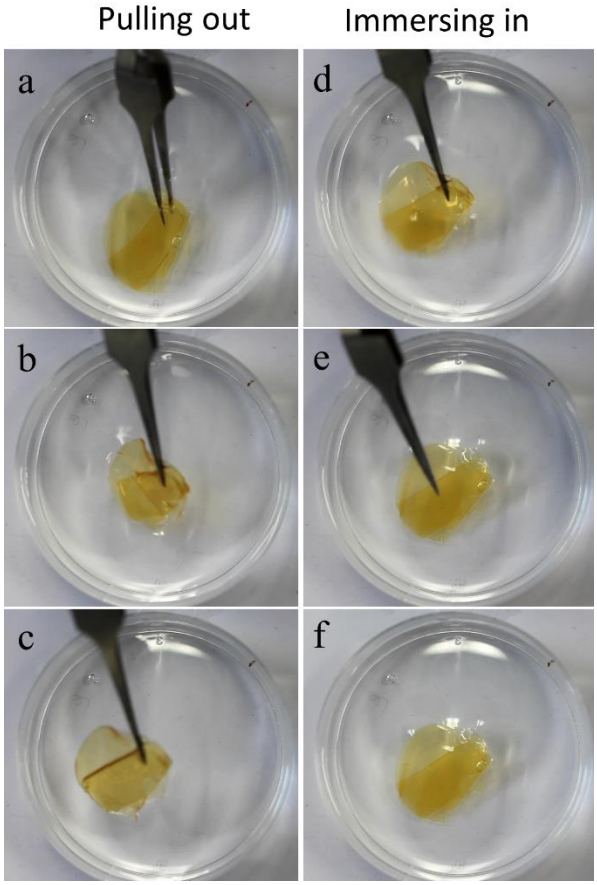

Figure S16: A ca. 800 µm thick [cALP-**S**$_1$] film, transferred across the water-air interface. It can be seen in panel [c], that the film does not self-fold when it is outside water.

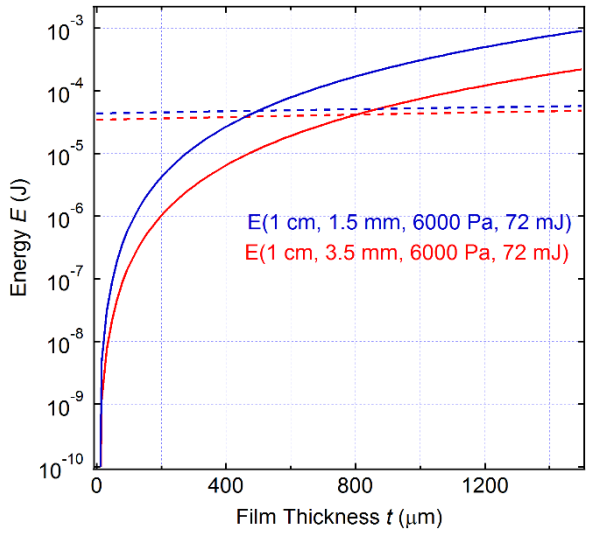

Figure S17: Theoretical calculation of elastic energies for crumpling (solid lines) and interfacial surface tension (dashed lines) for films having R= 1 cm, Y=6000 Pa, and r= 1.5 or 3.5 mm. It can be seen that the crossover of the both the energies occurs at around $t \approx$ 800 µm for a 1 cm radii completely spread film which folds into a ball of radius 3.5 mm.

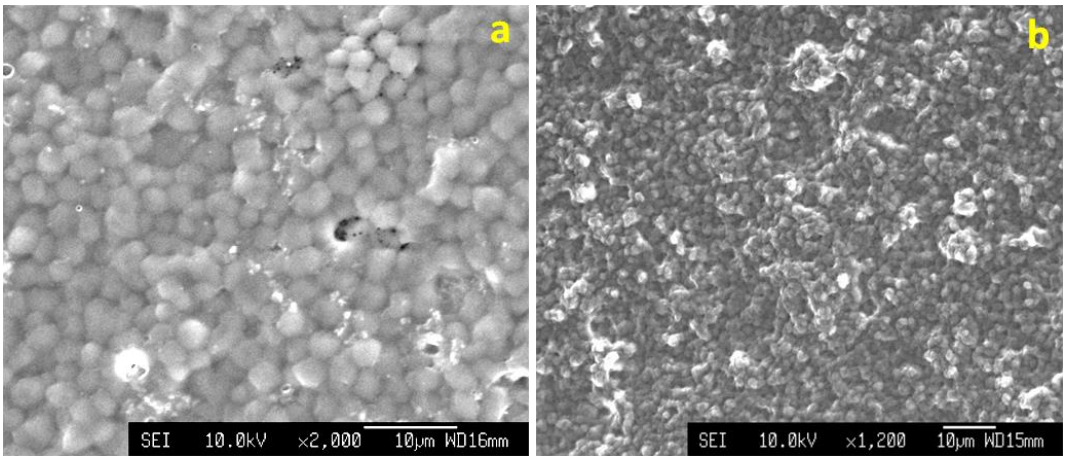

Figure S18: **SEM micrographs of hybrid films**: (a) [cMb-**S**$_1$] and (b) [cFn-**S**$_1$].

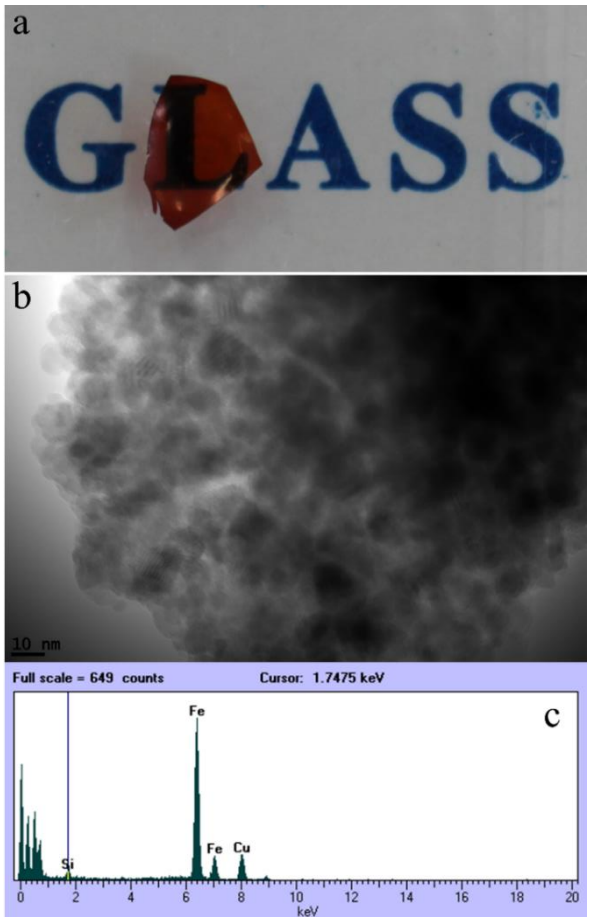

Figure S19: (a) A glass like solid and transparent of dry [cFn-**S**$_1$] film. (b) TEM of a 50 nm thick microtomed slice of [cFn-**S**$_1$] film showing the presence of agglomerated Ferritin molecules having the iron core intact as seen by the EDAX signal in (c).

Reference:

[1] M. -P. Pileni, *Adv. Colloid Interface Sci.* **1993**, *46*, 139.